

Diminished Surface Clustering and Increased Perinuclear Accumulation of Large Conductance Ca^{2+} -activated K^+ Channel in Mouse Myometrium with Pregnancy*

Received for publication, June 20, 2003, and in revised form, August 25, 2003
Published, JBC Papers in Press, September 2, 2003, DOI 10.1074/jbc.M306564200

Mansoureh Eghbali[‡], Ligia Toro^{§¶}, and Enrico Stefani^{‡¶¶}**

From the [‡]Department of Anesthesiology, Division of Molecular Medicine, the [§]Department of Molecular and Medical Pharmacology, the [¶]Department of Physiology, and the ^{¶¶}Brain Research Institute, David Geffen School of Medicine at University of California Los Angeles, Los Angeles, California 90095-1778

Large conductance Ca^{2+} -activated K^+ channels play a critical role in regulating myometrium contractility. Their current density, mRNA, and total protein are greatly diminished in myometrium of late pregnant rats versus nonpregnant animals. Opposite to rats, in mice, channel mRNA and total protein increase in late pregnancy, but current density decreases as in rats. Here, we investigated the mechanism of these differences. Real time PCR and Western blots demonstrate that, in late pregnancy, channel transcript quantities and total protein were diminished in rats but up-regulated in mice. High resolution confocal microscopy of single myocytes showed that, in nonpregnant mice, channels were expressed in clusters at the surface membrane. In late pregnancy, although there was an overall increase in channel protein, its majority was accumulated in perinuclear organelles, and channel clustering practically disappeared from the surface membrane. This contrasts with rat myometrium, where there is a reduction of channel transcripts and overall protein levels including the surface membrane. We conclude that large conductance Ca^{2+} -activated K^+ channel surface expression is reduced in both rat and mouse late pregnant myometrium. However, in rats, the main mechanism for the reduced channel expression at the cell surface is a diminished transcription, whereas in mice, it is an altered traffic to the surface.

Large conductance Ca^{2+} -activated K^+ (MaxiK)¹ channels play a critical role in myometrium contractility by regulating membrane potential and intracellular Ca^{2+} . MaxiK channels are highly expressed in uterine smooth muscle as a MaxiK channel-specific blocker, iberiotoxin, blocks the majority of outward K^+ currents in myometrial cells from nonpregnant rats (1–4). We have previously shown that in rats, myometrium MaxiK protein, both surface and total, and its mRNA levels are drastically diminished toward the end of pregnancy (4). In

contrast, work performed in mouse myometrium showed the opposite, that total protein of crude membrane preparations and mRNA increase in late pregnancy (5). However, in both rats (6) and mice (5), MaxiK current density that measures channel functional expression at the cell surface is diminished in late pregnancy. The reduction of MaxiK current density in late pregnant mice, regardless of its increase in total protein, was explained by a hypothetical change in the open probability of the channel via altered voltage/ Ca^{2+} sensitivities (5). Here, we investigated the mechanism that controls MaxiK current density by systematically comparing in rats versus mice and nonpregnant versus late pregnant myometrium MaxiK mRNA quantities in conjunction with MaxiK protein levels and its subcellular distribution. Consistent with previous findings (4, 5), our results show that MaxiK mRNA and total protein levels change in opposite directions, being reduced in late pregnant rats but increased in late pregnant mice. However, high resolution confocal microscopy of single uterine myocytes showed that in late pregnant mice the up-regulated MaxiK protein was accumulated in perinuclear organelles with a lower MaxiK protein density at the surface membrane. Most importantly, MaxiK channels were forming distinct clusters at the surface membrane in nonpregnant myometrium that practically disappeared during late pregnancy. These observations indicate that in both rats and mice, MaxiK channel density at the plasma membrane of myometrial cells is reduced toward the end of pregnancy, preparing myometrium for delivery. However, the molecular mechanism underlying this effect is radically different in rats and mice. In rats, transcriptional down-regulation and associated diminished protein levels can explain the surface MaxiK channel reduction. In mice, the reduction of surface MaxiK channel expression is not correlated with MaxiK transcript and protein down-regulation, but it appears to be mainly due to altered channel trafficking, since high levels of MaxiK channel protein were localized in perinuclear organelles.

EXPERIMENTAL PROCEDURES

Nonpregnant (NP; diestrus) and late pregnant (LP) rats (Sprague-Dawley) and mice (C57/BL) were used. Rats were 21–22 days pregnant, and mice were 19–20 days. Protocols received institutional review committee approval.

Real Time PCR—Total RNA was isolated from NP and LP rat and mouse myometrium using the ToTALLY™ RNA isolation kit (Ambion). Poly(A)⁺ RNA was purified using the Oligotex™ mRNA purification system (Qiagen). Purified mRNA (20 ng) was reverse transcribed to single-stranded cDNA by priming with oligo(dT) (avian myeloblastosis virus; Roche Applied Science). The quality of cDNA was confirmed by the lack of detectable genomic DNA using primers flanking intronic regions of β -actin (forward primer, 5'-GGCTACAGCTCACCACCAC-3', nucleotides 2383–2402; reverse primer, 5'-TACTCTGCTTGCT-GATCCAC-3', nucleotides 3071–3091, GenBank™ accession number V01217). Real time PCR (iCycler iQ Real Time PCR, Bio-Rad) was used

* This work was supported by National Institutes of Health Grants HL47382 and HL54970 (to L. T.) and HD38983 (to E. S.) and a Fellowship from the American Heart Association (to M. E.). The costs of publication of this article were defrayed in part by the payment of page charges. This article must therefore be hereby marked "advertisement" in accordance with 18 U.S.C. Section 1734 solely to indicate this fact.

** To whom all correspondence should be addressed: UCLA School of Medicine, Dept. of Anesthesiology, BH-520A CHS, Box 957115, Los Angeles, CA 90095-7115. Tel.: 310-794-7808; Fax: 310-825-6649; E-mail: estefani@ucla.edu.

¹ The abbreviations used are: MaxiK, large conductance and Ca^{2+} -activated K^+ ; NP, nonpregnant; LP, late pregnant; GAPDH, glyceraldehyde-3-phosphate dehydrogenase; dF/dT, temperature derivative of fluorescence; C_t , threshold cycle; PSF, point spread function.

for quantification of MaxiK and glyceraldehyde-3-phosphate dehydrogenase (GAPDH) cDNA using SYBRgreen I (diluted at 1:80,000 from stock solution $\times 10,000$) (Molecular Probes, Inc., Eugene, OR) and Platinum Quantitative PCR SuperMix-udg (Invitrogen). Measurements were performed in triplicate. Controls included the reaction mixture without cDNA or plasmid DNA and transcript levels of the housekeeping gene, GAPDH. Specific primers were designed to have a similar melting point and to amplify segments of ~200 base pairs of MaxiK and GAPDH. Specific products were detected as clear single peaks at their melting temperature in the first derivative of fluorescence (dF/dT) versus temperature plot (melting curve). As expected from the melting curve, a single band of the expected size was detected in agarose gel electrophoresis at the end of the reaction. Gene-specific primers were as follows: for MaxiK, forward primer 5'-CCATTAAGTCGGGTGATT-TAAG-3' (nucleotides 2515–2537) and reverse primer 5'-CCTTGG-GAATTAGCCTGCAAGA-3' (nucleotides 2681–2702); for GAPDH, forward primer 5'-TCCTGCACCACCACTGCTTAG-3' (nucleotides 1294–1315) and reverse primer 5'-GATGACCTTGCCACAGC-CTTG-3' (nucleotides 1485–1506) according to GenBank™ accession numbers U55995 (MaxiK) and AF106860 (GAPDH). The reaction conditions were as follows: 5 min at 95 °C followed by 40 cycles at 95 °C for 45 s, 61 °C for 45 s, and 72 °C for 45 s. GAPDH and MaxiK calibration curves were obtained using known concentrations of MaxiK (full-length clone) and GAPDH (200-bp amplicon). To obtain the standard curve, a threshold was assigned in the linear range of the fluorescence cycle number plot and plotted as a function of [cDNA]. The data were fitted to a straight line, where its slope is an indication of the reaction efficiency, and a slope of 3.32 represents 100% efficiency.

Antibodies—Rabbit polyclonal antibody raised against a purified peptide corresponding to residues 883–896 (GenBank™ accession number U11058) of the human MaxiK channel α subunit (anti- $\alpha_{883-896}$ antibody) and a commercial antibody (Alomone Laboratories) raised against a glutathione S-transferase fusion protein corresponding to residues 1098–1196 (GenBank™ accession number A48206) (anti- $\alpha_{1098-1196}$ antibody) were used. Both antibodies recognize rat and mouse MaxiK channels and can be blocked with the corresponding antigens. Vinculin monoclonal antibody was from Sigma.

Myometrium Membrane Preparation and Western Blots—After scraping off the endometrium, the myometrium was homogenized in 20 mM HEPES-KOH, 1 mM EDTA, 250 mM sucrose, pH 7.4, supplemented with 0.1 mM phenylmethylsulfonyl fluoride, 1 μ M pepstatin A, 1 μ M/ml aprotinin, and 1 μ M/ml leupeptin. The homogenate was centrifuged at $1,000 \times g$ for 15 min, and the supernatant was then centrifuged at $100,000 \times g$ for 30 min to obtain crude membranes. Membranes were suspended in 250 mM sucrose, 10 mM HEPES-KOH, pH 7.4, and treated with SDS loading buffer and dithiothreitol to a final concentration of 62.5 mM Tris-Cl, 2% SDS, 10% glycerol, 0.01% bromophenol blue, and 42 mM dithiothreitol and stored at -70 °C. Protein concentration was measured using the Bradford method (Pierce). Prestained molecular weight standards were from Invitrogen or from Li-Cor. Myometrial membrane proteins (5–40 μ g) were separated by 6–10% SDS-polyacrylamide gels under reducing conditions and electrotransferred to nitrocellulose paper. Blots analyzed with chemiluminescence were blocked with Tris-buffered saline (TBS; 50 mM Tris-HCl, 150 mM NaCl, 0.5% Triton X-100, and 0.1% Tween, pH 7.4) containing 5% nonfat dry milk for 1 h at room temperature. Thereafter, they were incubated with primary antibodies: anti- $\alpha_{883-896}$ (0.8 μ g/ml) or anti- $\alpha_{1098-1196}$ (6 μ g/ml) and anti-vinculin (0.43 μ g/ml) antibodies in 1% nonfat milk/TBS for 12 h at 4 °C, washed with TBS three times for 10 min each, and then incubated with horseradish peroxidase-conjugated secondary antibody for 1 h, Alexa Fluor 680 goat anti-rabbit IgG (0.133 μ g/ml) (Molecular Probes), or IRDye™ 800 goat anti-mouse (0.066 μ g/ml) (Rockland, Inc.) for 1 h. After washing, blots were treated for 1 min with chemiluminescence Reagent Plus (PerkinElmer Life Sciences) and autoradiographed on Eastman Kodak Co. BioMax film. Alternatively, to achieve a wider dynamic range for relative quantification, blots were developed using the Odyssey infrared imaging system (Li-Cor). In this case, the blocking solution was without detergent. Direct infrared detection makes it possible to detect strong and weak bands on the same blot and to perform dual labeling. Western blots showed two bands at an approximately equivalent position that were identified as being MaxiK channel protein. The specificity of the antibody was tested by preadsorbing with the antigenic peptide (3–10 mg of peptide/mg of antibody). Bands corresponding to the immunoreactive MaxiK protein (estimated molecular mass ~120 kDa) were quantified using the BioRad GS670 Imaging Densitometer (for chemiluminescence) or with MetaMorph (Universal Imaging Corp.) (for infrared fluorescence). Results are expressed as pixel intensity.

Cell Isolation—The uterus was quickly removed and placed in ice-cold dissociation solution containing 55 mM NaCl, 6 mM KCl, 5 mM $MgCl_2$, 10 mM HEPES, 10 mM glucose, 80 mM sodium glutamate, pH 7.4. The endometrial layer was peeled off, and the myometrium was cut into small square pieces (2×2 mm). Papain 38 units/ml (Sigma) was preactivated in dissociation solution with 0.22 mM EDTA and 2.2 mM dithiothreitol for 20 min. Collagenase stock solution, 10,128 units/ml (Type IA; Sigma) was prepared in dissociation solution with 2 mM $CaCl_2$. Collagenase was then added to the preactivated papain solution to a final concentration of 1,030 units/ml collagenase, 33.6 units/ml papain, 0.2 mM Ca^{2+} , 0.2 mM EDTA, 2 mM dithiothreitol. The myometrium pieces were incubated in this mixture in a shaking water bath at 25 °C for 40–60 min. After washing three times with dissociation solution, single cells were obtained by gentle trituration of the digested tissue with a plastic pipette. Cells were washed and resuspended in the dissociation solution, plated on coverslips precoated with laminin (20 μ g/ml) for 1 h, and fixed for immunocytochemistry.

Immunocytochemistry—Stretched uteri or freshly dissociated myometrium cells were fixed in 4% paraformaldehyde, 2% picric acid in 0.1 M Na_2HPO_4 , adjusted to pH 7.4 with NaH_2PO_4 for 2 h for whole tissue or 20 min for isolated cells. Nonspecific binding was blocked by incubating the transverse cryostat sections (10 μ m) or isolated cells with 5% donkey serum for 30 min at room temperature. The tissue sections or isolated cells were incubated for 12 h at 4 °C with anti- $\alpha_{1098-1196}$ antibody (3 μ g/ml) in 0.5% normal donkey serum, 0.2% Triton X-100 in PBS: 10 mM Na_2HPO_4 , 2.3 mM NaH_2PO_4 , 138 mM NaCl, and 2.7 mM KCl, pH 7.4, washed with 0.2% Triton X-100 in PBS three times for 5 min each, and then incubated with 7.5 μ g/ml Rhodamine Red™-X-conjugated affinity-purified donkey anti-rabbit IgG (Jackson ImmunoResearch Laboratories, Inc.) for 1 h at room temperature. Tissue sections or isolated cells were washed in PBS three times for 5 min each and mounted using Prolong (Molecular Probes). The specificity of the antibody was tested by preadsorbing with the antigen (5 mg/mg antibody). NP and LP pregnant samples were stained in parallel, and confocal images were taken with the same laser intensity. Stacks of images were typically acquired by optically sectioning tissues or cells every 0.25 μ m at 0.115 μ m per pixel with a confocal microscope (Olympus Fluoview). Images were analyzed using Image-Pro Plus (Media Cybernetics), MetaMorph (Universal Imaging Corp.), and Auto Deblur (AutoQuant).

Digital Image Processing: Three-dimensional-Blind Deconvolution—Confocal images show out of focus fluorescence due to intrinsic optical nonuniformities; nevertheless, they can be significantly improved by image processing (7). The processing involves the characterization of the out of focus signals and their removal from the acquired images. This process is generally referred to as deconvolution or image restoration. The characterization of out-of-focus signal is based on the three-dimensional image of a point source of light, the so-called point-spread function (PSF). The deconvolution process should remove the out of focus information transforming diffuse PSF in a single point PSF (8). Fig. 1 illustrates the PSF of 0.1 μ m fluorescein isothiocyanate-fluorescent beads (Molecular Probes) obtained for the laser-scanning confocal microscope used in our studies (Olympus Fluoview, $\times 60$, 1.4 numerical aperture, oil immersion). Stacks of images were acquired every 0.1 μ m in the z axis at 0.057 μ m/pixel in the x, y plane. The images at the left show unprocessed signals with the ovoid shape PSF typical for laser-scanning confocal microscopy (9). The images at the right show the result of applying three-dimensional-blind deconvolution with Auto-Deblur (AutoQuant) (10). This method uses an image reconstruction algorithm applying the “maximum likelihood” to search for the PSF in the acquired data that caused the acquired image. This process increases the resolution practically to the theoretical limit in the y, x axis (top panels); z, x axis (lower panels); and z, y axis (not shown) and was used for image analysis of MaxiK localization in isolated myometrial cells from NP and LP mice.

Statistics—Unless otherwise stated, data were expressed as mean \pm S.E. Comparisons between two groups were analyzed by Student's t test with a statistical significance of <0.05 .

RESULTS

MaxiK Transcripts Are Down-regulated in Rats and Up-regulated in Mice at the End of Pregnancy—Using an RNA protection assay, we have previously shown that, in LP rats, myometrium MaxiK transcripts were down-regulated (4), whereas Benkusky *et al.* (5) found that, in LP mouse, myometrium MaxiK transcripts were up-regulated. As a first step, to understand these differences, we used real time PCR as an

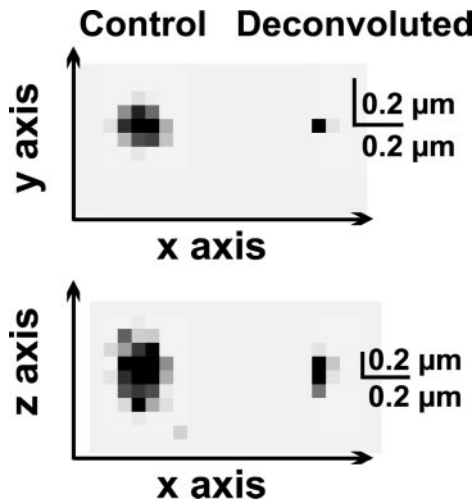


FIG. 1. Laser confocal microscopy resolution at the theoretical limit after three-dimensional-blind deconvolution. PSF for laser-scanning confocal microscopy before (left images) and after three-dimensional-blind deconvolution (right images). Top panel, y , x axis; bottom panel, z , x axis. PSF was obtained with $0.1 \mu\text{m}$ fluorescein isothiocyanate-fluorescent beads. Confocal sections were taken every $0.1 \mu\text{m}$ in the z axis and at $0.057 \mu\text{m}/\text{pixel}$ in the y , x axis. After three-dimensional-blind deconvolution, a resolution below $0.2 \mu\text{m}$ was achieved in the y , x axis and of about $0.5 \mu\text{m}$ in the z axis.

alternative method to systematically compare the pattern of MaxiK transcript expression in NP and LP rat and mouse myometrium and to quantify the absolute values of MaxiK transcripts. Fig. 2A shows the fluorescence intensity versus cycle number plot for 100, 10, 1, 0.1, 0.01, and 0.001 pg of MaxiK amplicon. The broken line marks the threshold used to construct the standard calibration curve in Fig. 2E (open circles). Fig. 2B shows the melting curve with a single sharp peak for all samples, indicating the presence of a single PCR product. The fluorescence cycle number curves for NP and LP rats are shown in Fig. 2C. The curve is right-shifted at the end of pregnancy (LP), indicating that MaxiK transcripts become less abundant at this gestational stage. Opposite to this finding, in myometrium from LP mouse, the MaxiK curve is left-shifted, demonstrating in this species an up-regulation of MaxiK transcripts at the end of pregnancy (Fig. 2D). The curves also show a higher abundance of MaxiK transcripts in NP rat myometrium than in NP mouse myometrium, as indicated by a lower threshold cycle number in rat versus mouse (19 versus 23). To calculate the absolute values of reverse transcribed MaxiK mRNA, we selected the same threshold value for all the samples in the linear range of the fluorescence versus cycle number curves (Fig. 2, C and D, broken lines) and interpolated them in the standard curve (Fig. 2E; ■, NP rat; □, LP rat; ▲, NP mouse; △, LP mouse). The results are summarized in Fig. 2F. The absolute MaxiK transcript values were (in pmol/g mRNA) for rats, 65 ± 7 in NP and 2 ± 0.6 in LP myometrium; and values for mice were 2.6 ± 0.8 in NP and 30 ± 7 in LP myometrium ($n = 3$). As control, GAPDH showed no significant change between NP and LP myometrium in both species. Consistent with previous RNA protection assay determinations, real time PCR experiments showed that indeed myometrium MaxiK transcripts are down-regulated in rats but up-regulated in mice at the end of pregnancy, indicating that the mechanism of MaxiK transcript hormonal regulation is different, depending on the species.

MaxiK Total Protein Is Down-regulated in Rats but Up-regulated in Mice at the End of Pregnancy—MaxiK protein quantification using Western blots of myometrial crude membrane preparations produced similar results as real time PCR experiments. Fig. 3A shows that anti- $\alpha_{1098-1196}$ antibody rec-

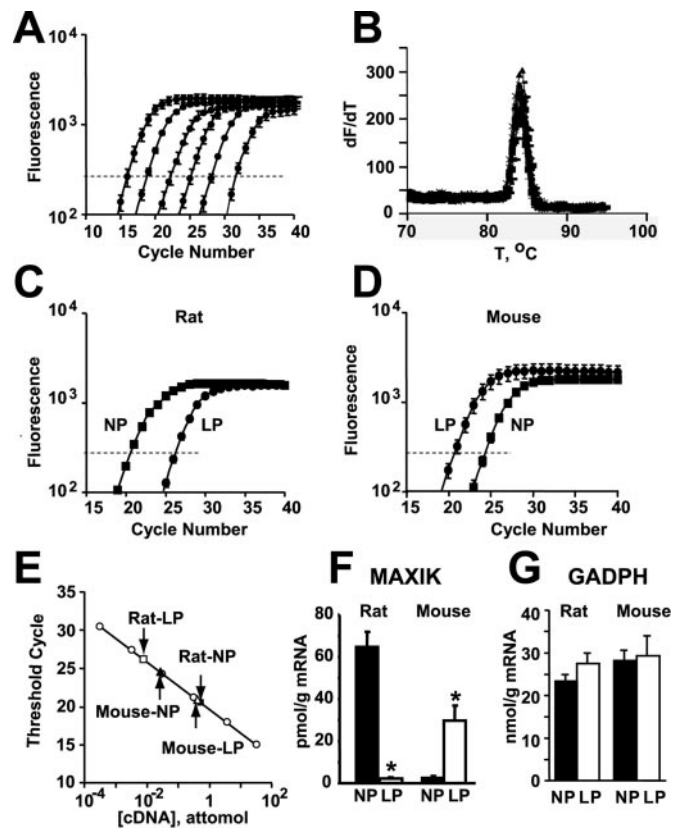


FIG. 2. MaxiK transcript is down-regulated in rats but up-regulated in mice at the end of pregnancy. A, fluorescence intensity versus cycle number for known quantities of MaxiK amplicon (from left to right: 100, 10, 1, 0.1, 0.01, and 0.001 pg). The broken line is the threshold used to obtain the MaxiK standard curve in E. B, overlapping melting curves for samples in A, C, and D. C and D, examples of fluorescence intensity versus cycle number plots for MaxiK in myometrium from NP (■) and LP (●) rats and mice. The error bars are from triplicates. E, standard calibration curve obtained by plotting the threshold cycle (dashed line in A) versus [cDNA]. Open circles, known concentrations of MaxiK cDNA. The solid line is the data fitted to a straight line with a slope of -3.2 . The arrows point to the absolute values of MaxiK transcripts in rats and mice (■, NP rat; □, LP rat; ▲, NP mouse; △, LP mouse). F, mean absolute values of MaxiK transcripts in rat and mouse, NP and LP myometrium ($n = 3$ real time PCR determinations, four cDNA preparations from seven animals in each condition). G, absolute values of myometrium GAPDH transcripts for experiments in C and D show no significant change in NP versus LP myometrium. Experiment done in triplicate. Similar results were obtained in at least four different experiments with different cDNAs in each condition.

ognizes in both rats and mice a doublet at approximately the expected molecular size of MaxiK channel protein (~ 125 kDa, arrows). This signal is specific, since the protein-antibody interaction was fully inhibited when the antibody was preadsorbed with the corresponding antigen ($10 \mu\text{g}/\text{ml}$; not shown). Different concentrations of membrane protein were loaded, and dose-response curves were constructed to compare the relative abundance of MaxiK in NP versus LP rats (Fig. 3B) and mice (Fig. 3C). Dose-response curves show that MaxiK protein is diminished in rats but increased in mice prior labor by about 3- and 8-fold, respectively. Qualitatively similar results were obtained in another four preparations. These results are in agreement with previous work and demonstrate opposite MaxiK protein handling in rats versus mice. However, the increase in total protein in LP mice cannot explain the previously reported decrease in MaxiK current density (5). Therefore, we examined the possibility that the subcellular distribution of MaxiK is different in NP versus LP mouse with less surface expression at the end of pregnancy.

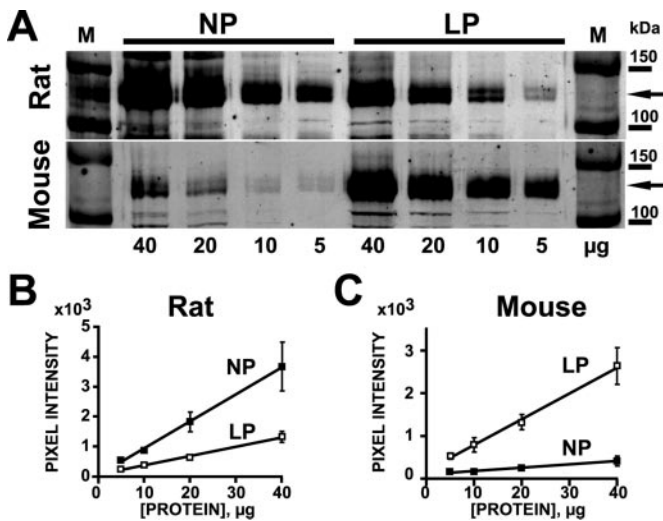


FIG. 3. MaxiK protein level is diminished in rat but increased in mouse myometrium at the end of pregnancy. *A*, Western blots of membrane fractions from NP and LP rat (*top blot*) and mouse (*lower blot*) labeling MaxiK channel protein at ~125 kDa (*arrows*). Contrast was increased to illustrate the low expression in NP mouse; however, signals were not saturated. *B* and *C*, pixel intensity *versus* protein concentration plots of blots in *A* showing a linear relationship. *Bars*, S.D. of mean pixel intensities. A similar trend was observed in another four preparations in each condition. Vinculin labeling of the same blots gave no difference in NP and LP myometrium in both rat and mouse ($n = 2$).

MaxiK Channel Protein Accumulates in Cytoplasmic Regions of Myometrial Cells from Late Pregnant Mice—Using immunocytochemistry, we have previously shown that during pregnancy there is a dramatic reduction in the overall MaxiK protein in rats including decreased surface expression and some degree of accumulation in the perinuclear region (4). However, the subcellular distribution of MaxiK protein in uterine myocytes from NP and LP mice is unknown. Tissue sections from NP and LP mouse myometrium were examined using anti- $\alpha_{1098-1196}$ antibody. Fig. 4 shows single confocal planes of transverse uterine sections illustrating the circular layer from NP (*A*) and LP (*B*) mice. Consistent with Western blots, the images in NP mouse showed very low levels of MaxiK signal that appeared to be mainly located at the surface membrane of smooth muscle cells (*arrows*). On the other hand, myometrium from late pregnant mice was strongly labeled with the MaxiK antibody (Fig. 4*B*), but the majority of the protein seemed accumulated in the cytoplasm in perinuclear organelles. No staining was detected when the anti-MaxiK antibody was preadsorbed with the corresponding antigen (Fig. 4*C*). Since, in confocal images of tissue sections, it was difficult to distinguish the level of immunostaining at the cell surface, we performed MaxiK immunostaining in freshly isolated myometrial cells. Fig. 5 illustrates a montage of raw single confocal planes near the middle of isolated myometrial cells from NP (*A*) and LP (*B*) mice. Note that in NP mice (*A*), MaxiK labeling shows some degree of clustering near the cell surface with very little intracellular labeling, whereas in LP mice there is an overall large increase in total MaxiK protein, which is mostly localized surrounding the nucleus (*B*). Although single cell labeling significantly increased the optical resolution when compared with tissue sections, analysis of middle sections could not determine whether MaxiK channel expression was different at the cell surface in NP *versus* LP uterine myocytes. Therefore, we further analyzed stacks of images taken every 0.25 μm in the *z* plane.

MaxiK Channel Localizes in Clusters at the Surface of NP Mouse Uterine Myocytes and Redistributes in Late Pregnancy—

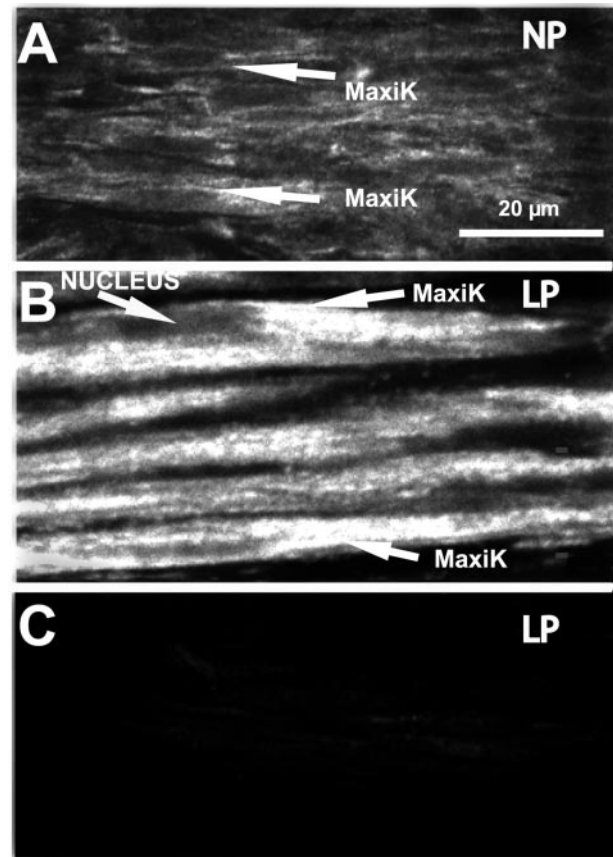


FIG. 4. MaxiK channel protein accumulation in cytoplasmic regions of myometrial cells of late pregnant mouse. Single confocal planes of transverse uterine sections illustrating the circular layer from NP and LP mouse stained with anti- $\alpha_{1098-1196}$ antibody. *A*, NP, the *arrows* mark plasma membrane expression. *B*, LP, the *arrows* mark nuclear region and MaxiK cytoplasmic expression. *C*, block of MaxiK signal after antibody preincubation with the antigen.

In order to determine whether the degree of MaxiK labeling at the cell surface is different in myometrial cells from NP and LP mice, stacks of confocal images were restored with three-dimensional-blind deconvolution. Fig. 6 shows bright field differential interference contrast images and the corresponding deconvoluted confocal middle sections of NP (*A* and *C*) and LP (*B* and *D*) uterine myocytes. Note that in the NP myocyte (*C*), MaxiK channels seem clustered at the surface membrane where the optical section is close to the surface (*arrows*). On the other hand, in the LP uterine myocyte (*D*), MaxiK channel clustering was barely detected at the periphery, and the protein is mainly visualized in canaliculate type structures throughout the cytoplasm with predominant staining near the nucleus (*D*, *inset*). *E–H* illustrates the analysis of optical sections at the top of NP and LP cells corresponding to the cell plasma membrane. *E* is a raw image of a confocal section near the top surface of a cell of NP myometrium, and *F* is after image restoration. Note in *F*, after deconvolution, the clear clustered pattern of MaxiK channel localization. *G* illustrates the region depicted in *F* (*square*) at a higher magnification. On the other hand, LP uterine myocytes show an overall reduction of MaxiK channel labeling at the cell surface without a noticeable clustering. As an example, *H* illustrates the region in *B* at higher magnification and taken at the top surface after deconvolution, demonstrating the lack of detection of MaxiK channel clusters. This is quantified in Fig. 7, which shows the line scan plot between the *arrows* in Fig. 6, *F* and *H*. The plot reflects the regular peak pattern of the clusters at the cell surface in the NP uterine myocyte (■) and the smooth and lower intensity

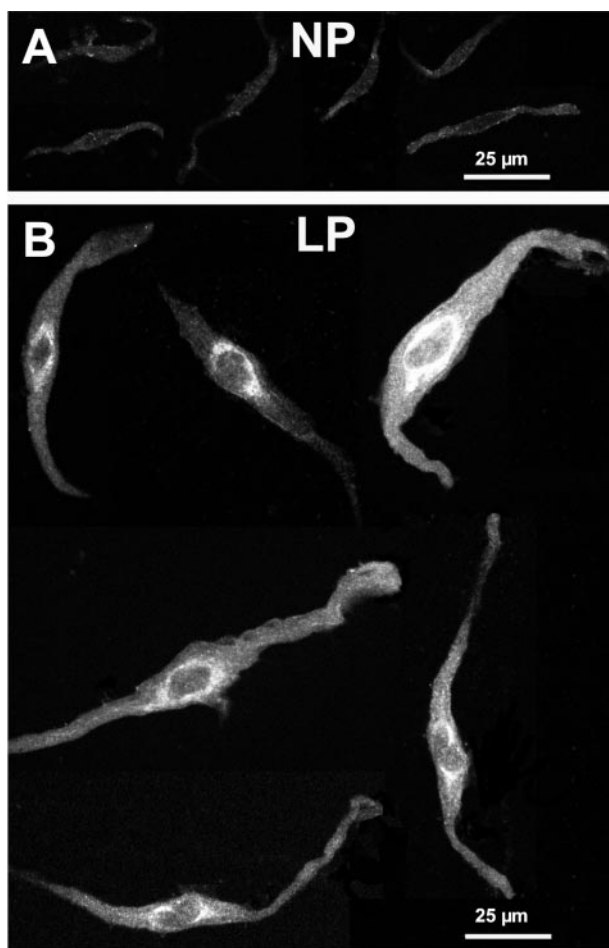


FIG. 5. MaxiK channel protein accumulation in perinuclear organelles in isolated uterine cells at term. Shown are single confocal images near the middle of the cells from isolated uterine smooth muscle cells from NP (A) and LP (B) mouse. The cells were immunostained with anti- $\alpha_{1098-1196}$ antibody. Note the weaker stain of NP cells when compared with LP cells and the strong MaxiK cytoplasmic staining in the perinuclear region of LP cells.

signal in the LP myocyte (\square). Cluster analysis in a NP myocyte after setting the lower threshold at 100-pixel intensity (Fig. 7, broken line) gives the following cluster values: cluster area $0.083 \pm 0.011 \mu\text{m}^2$, estimated radius $160 \pm 15 \text{ nm}$, and $0.72 \text{ clusters}/\mu\text{m}^2$ ($n = 43$ clusters). Similar results were obtained in another seven LP and NP uterine myocytes. We can conclude that MaxiK channels in NP uterine myocytes are localized in discrete microdomains, forming clusters at the cell surface that are difficult to distinguish in LP myometrium. The disappearance of MaxiK channel from the cell surface and the increased protein accumulation in the perinuclear region at the end of pregnancy reconcile the increase in total protein measured with Western blot with the decreased current density that reflects the active channels at the surface membrane in LP mouse.

DISCUSSION

The main findings of this work are that 1) MaxiK transcripts and total protein are diminished in rats but up-regulated in mice at the end of pregnancy; 2) despite an overall increase in total protein in mice at the end of pregnancy, there is little signal at the surface membrane; 3) in LP mouse myocytes, the majority of the protein appears to be in the cytoplasm in a canalicular pattern that is more evident near the nucleus; and 4) MaxiK channels in NP mice are localized in discrete microdomains, forming clusters at the cell surface that are difficult to distinguish in LP myometrium.

During pregnancy, the uterine smooth muscle undergoes dramatic changes in hormonal levels, morphology, and state of contractile activity. Electrophysiological recordings in both rats and mice indicate that the majority of K^+ outward current in NP uterine smooth muscle cells is due to the activity of MaxiK channels, since the majority of the outward current was blocked by iberiotoxin (4, 5). MaxiK channels are also present in LP mice and rats (5, 6, 11) but seem to contribute less to the total outward K^+ current. The lower current density of MaxiK channel in rats correlated well with our findings showing that the MaxiK transcript and total and surface protein are drastically decreased toward the end of pregnancy (4). However, the lower MaxiK current density in mice could not be explained from the total protein and transcript measurements, since both are increased at the end of pregnancy (5). The diminution of MaxiK channel function at the end of pregnancy in mouse was attributed to 1) a hypothetical lower Ca^{2+} sensitivity of the channel, 2) a potential right shift in the channel activation curve, 3) different regulation of MaxiK channel splice variants during pregnancy, and 4) up-regulation of the accessory β_1 subunit (5, 6, 12, 13). In this work, using image restoration of confocal images, we found that although at the end of pregnancy there is an overall increase in total protein in mice, the majority of the protein is accumulated in the cytoplasm with little signal at the surface membrane. It appears that a novel mechanism that involves altered channel trafficking during pregnancy can explain the lower ionic current measurements despite an increase in total protein (5). Previous immunocytochemistry experiments in rats also showed that although MaxiK surface protein is diminished in myometrium close to term, the small amount synthesized is accumulated in the perinuclear region (4). Similarly, Kv4.3 down-regulation in rat myometrium at term is associated with perinuclear accumulation of Kv4.3 protein (14). Therefore, a diminished intracellular traffic in both rats and mice may modulate surface expression of channel proteins in LP myometrium. This mechanism seems to be predominant in mouse myometrium near term, explaining the reduced surface expression of MaxiK channel. Our results also indicate that during pregnancy there are species differences in the way MaxiK channel mRNA and total protein are expressed and handled. In rats, there is a parallel correspondence between surface protein and mRNA levels, suggesting that the predominating mechanism regulating MaxiK channel protein expression is transcription (4). This contrasts with mice, where traffic regulation seems to be the predominant mechanism. Since during pregnancy there are dramatic changes in sex hormone levels, we may speculate that sex hormones may diminish channel traffic to the surface, a mechanism that seems to be predominant in mouse myometrium.

To our knowledge, this work presents the first direct evidence that MaxiK channels are not evenly distributed at the surface membrane of smooth muscle cells but are localized in microdomains, forming clusters. Recent evidence suggests that channel clustering forming macromolecular complexes with regulatory signaling enzymes seems necessary to create localized cell machineries dedicated to specific cell functions. For example, L-type Ca^{2+} channels colocalizes in puncta with β_2 adrenergic receptor in hippocampal axosomatic synapses for synaptic function (15) and with ryanodine receptors and calsequestrin in heart cells for excitation-contraction coupling (16), and Kv2.1 K^+ channels spatially associate in clusters with ryanodine receptors regulating dendritic Ca^{2+} transients (17). In smooth muscle from cerebral arteries, MaxiK channels are functionally coupled to ryanodine receptors via Ca^{2+} sparks, which activate MaxiK channels favoring relaxation (18). In

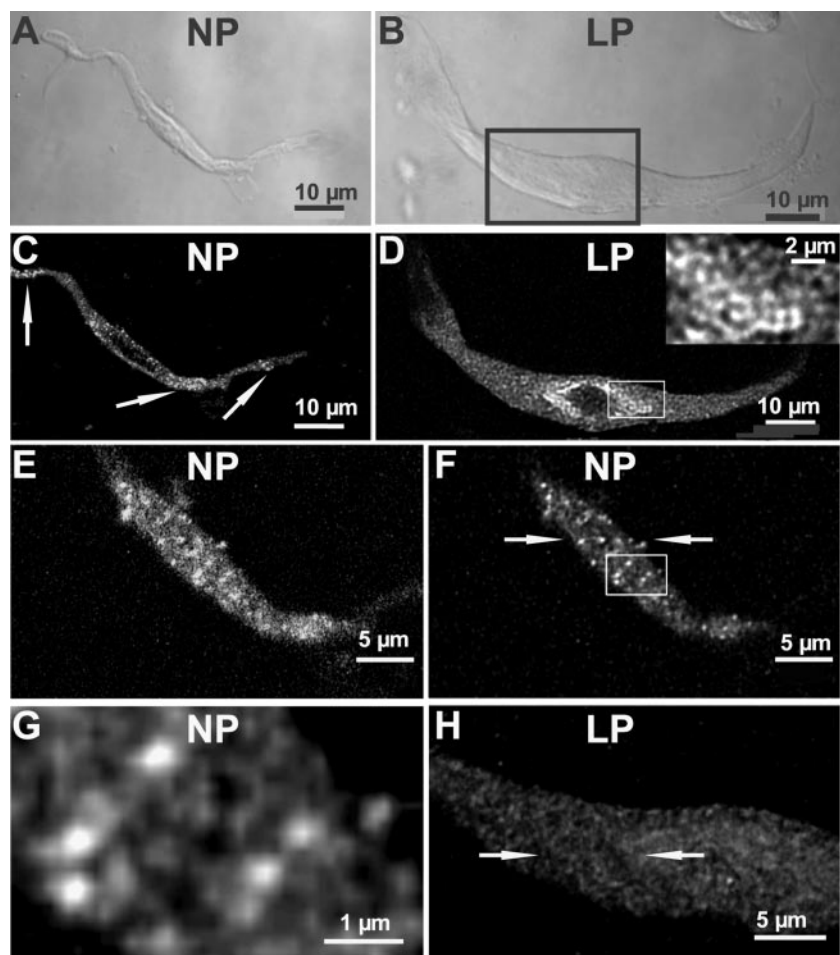


FIG. 6. MaxiK channel clustering at the surface membrane in uterine myocytes from NP mouse. Bright field differential interference contrast images and the corresponding deconvoluted confocal middle sections of NP (A and C) and LP (B and D) uterine myocytes. C, note MaxiK channel clustering in the periphery of the nuclear region and their localization at the surface membrane in regions where the optical section is close to the surface (arrows). D, MaxiK channel protein is mainly visualized in canalicular type structures throughout the cytoplasm with predominant staining near the nucleus (inset at higher magnification). E and F, raw and three-dimensional-blind deconvoluted images from a confocal section near the top surface of a NP cell. Note the MaxiK clustered pattern at the surface. G, region depicted in F at higher magnification. H, region depicted in B at the top surface after three-dimensional-blind deconvolution. Note the lack of MaxiK channel clusters in LP uterine myocytes.

agreement with our MaxiK clustering measurements, recent Ca^{2+} sparks data in amphibian smooth muscle suggest that MaxiK channels do not appear to be uniformly distributed over the membrane, but instead they may form clusters at the spark site with an estimated radius of 150–300 nm for the membrane area over which a Ca^{2+} concentration $\geq 10 \mu\text{M}$ is reached to activate MaxiK channels (19). This local Ca^{2+} concentration is optimal to fully activate MaxiK channels assembled by the pore-forming α subunit and its β_1 regulatory subunit (20). Thus, our results showing MaxiK clusters at the surface membrane with an estimated radius of about 200 nm are in agreement with functional studies and support the view that MaxiK channels form distinct and localized macromolecular complexes optimized for its function that can undergo remodeling in late pregnancy.

In conclusion, surface expression of MaxiK channel protein can be influenced by transcriptional regulation and intracellular trafficking probably under the control of sex hormones during pregnancy. Our results demonstrate that in both mice and rats the final result at the end of pregnancy is a diminished surface expression of MaxiK channel protein that would translate to a higher myometrium contractility favoring parturition.

Acknowledgment—We thank Dr. Min Song for Western blot analysis.

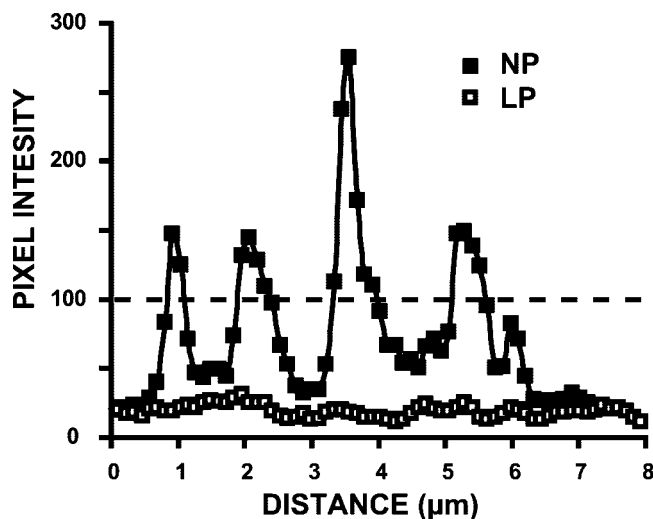


FIG. 7. Line scan plot of MaxiK channel clusters in NP uterine myocytes. Line scan plot between the arrows in Fig. 6 for a NP (F) and LP (H) uterine myocytes. Note the regular pattern of the peaks (clusters) in the NP uterine myocyte (■) and the smooth and lower intensity plot in the LP myocyte (□). The broken line marks the lower threshold (100-pixel intensity) used for cluster analysis (values given under "Results").

REFERENCES

1. Anwer, K., Oberti, C., Pérez, G. J., Perez-Reyes, N., McDougall, J. K., Monga, M., Sanborn, B. M., Stefani, E., and Toro, L. (1993) *Am. J. Physiol.* **265**, C976–C985
2. Candia, S., Garcia, M. L., and Latorre, R. (1992) *Biophys. J.* **63**, 583–590
3. Galvez, A., Gimenez-Gallego, G., Reuben, J. P., Roy-Contancin, L., Feigenbaum, P., Kaczorowski, G. J., and Garcia, M. L. (1990) *J. Biol. Chem.* **265**, 11083–11090
4. Song, M., Zhu, N., Olcese, R., Barila, B., Toro, L., and Stefani, E. (1999) *FEBS Lett.* **460**, 427–432
5. Benkusky, N. A., Fergus, D. J., Zuccherro, T. M., and England, S. K. (2000) *J. Biol. Chem.* **275**, 27712–27719
6. Wang, S. Y., Yoshino, M., Sui, J. L., Wakui, M., Kao, P. N., and Kao, C. Y. (1998) *J. Gen. Physiol.* **112**, 737–756
7. Shaw, P. J. (1995) in *Handbook of Biological Confocal Microscopy* (Pawley, J. B., ed) pp. 373–387, Plenum, New York
8. McNally, J. G., Karpova, T., Cooper, J., and Conchello, J. A. (1999) *Methods* **19**, 373–385
9. Andrews, P. D., Harper, I. S., and Swedlow, J. R. (2002) *Traffic* **3**, 29–36
10. Holmes, T. J., and O'Connor, N. J. (2000) *J. Microsc.* **200**, 114–127
11. Perez, G. J., Toro, L., Erulkar, S. D., and Stefani, E. (1993) *Am. J. Obstet. Gynecol.* **168**, 652–660
12. Benkusky, N. A., Korovkina, V. P., Brainard, A. M., and England, S. K. (2002) *FEBS Lett.* **524**, 97–102
13. Holdiman, A. J., Fergus, D. J., and England, S. K. (2002) *Mol. Cell. Endocrinol.* **192**, 1–6
14. Song, M., Helguera, G., Eghbali, M., Zhu, N., Zarei, M. M., Olcese, R., Toro, L., and Stefani, E. (2001) *J. Biol. Chem.* **276**, 31883–31890
15. Davare, M. A., Avdonin, V., Hall, D. D., Peden, E. M., Burette, A., Weinberg, R. J., Horne, M. C., Hoshi, T., and Hell, J. W. (2001) *Science* **293**, 98–101
16. Scriven, D. R., Dan, P., and Moore, E. D. (2000) *Biophys. J.* **79**, 2682–2691
17. Antonucci, D. E., Lim, S. T., Vassanelli, S., and Trimmer, J. S. (2001) *Neuroscience* **108**, 69–81
18. Nelson, M. T., Cheng, H., Rubart, M., Santana, L. F., Bonev, A. D., Knot, H. J., and Lederer, W. J. (1995) *Science* **270**, 633–637
19. ZhuGe, R., Fogarty, K. E., Tuft, R. A., and Walsh, J. V., Jr. (2002) *J. Gen. Physiol.* **120**, 15–27
20. Meera, P., Wallner, M., Jiang, Z., and Toro, L. (1996) *FEBS Lett.* **382**, 84–88